

Cite this: *Chem. Sci.*, 2017, 8, 6117

## On the incompatibility of lithium–O<sub>2</sub> battery technology with CO<sub>2</sub>†

Shiyu Zhang,<sup>†a</sup> Matthew J. Nava,<sup>†a</sup> Gary K. Chow,<sup>b</sup> Nazario Lopez,<sup>†a</sup> Gang Wu,<sup>c</sup> David R. Britt,<sup>b</sup> Daniel G. Nocera<sup>\*,d</sup> and Christopher C. Cummins<sup>\*,a</sup>

When solubilized in a hexacarboxamide cryptand anion receptor, the peroxide dianion reacts rapidly with CO<sub>2</sub> in polar aprotic organic media to produce hydroperoxycarbonate (HOOCO<sub>2</sub><sup>-</sup>) and peroxydicarbonate (<sup>-</sup>O<sub>2</sub>COOCO<sub>2</sub><sup>-</sup>). Peroxydicarbonate is subject to thermal fragmentation into two equivalents of the highly reactive carbonate radical anion, which promotes hydrogen atom abstraction reactions responsible for the oxidative degradation of organic solvents. The activation and conversion of the peroxide dianion by CO<sub>2</sub> is general. Exposure of solid lithium peroxide (Li<sub>2</sub>O<sub>2</sub>) to CO<sub>2</sub> in polar aprotic organic media results in aggressive oxidation. These findings indicate that CO<sub>2</sub> must not be introduced in conditions relevant to typical lithium–O<sub>2</sub> cell configurations, as production of HOOCO<sub>2</sub><sup>-</sup> and <sup>-</sup>O<sub>2</sub>COOCO<sub>2</sub><sup>-</sup> during lithium–O<sub>2</sub> cell cycling will lead to cell degradation *via* oxidation of organic electrolytes and other vulnerable cell components.

Received 17th March 2017  
Accepted 19th June 2017

DOI: 10.1039/c7sc01230f

rsc.li/chemical-science

### Introduction

The two-electron reduction of molecular oxygen to the peroxide dianion is an attractive cathode redox couple for developing rechargeable lithium–O<sub>2</sub> batteries.<sup>1</sup> Lithium carbonate (Li<sub>2</sub>CO<sub>3</sub>) formation is deleterious to battery performance because it passivates electrodes and causes a drastic reduction in the round trip efficiency of discharge–charge cycles.<sup>2,3</sup> Carbonate formation is typically ascribed to oxidative degradation of organic electrolytes<sup>4–6</sup> and carbon electrodes<sup>7</sup> by superoxide<sup>8,9</sup> and singlet oxygen.<sup>10</sup> Although peroxide is often considered to be a strong oxidant in aqueous media, salts of its dianion (O<sub>2</sub><sup>2-</sup>) are poor oxidizers in organic media due to their extremely low solubility and so, for this reason, the possible role of peroxide in furnishing carbonate is underappreciated.<sup>11</sup> The presence of

carbonate-derived CO<sub>2</sub> during the recharge cycle of lithium–O<sub>2</sub> batteries<sup>2</sup> prompted us to consider the possibility that carbonate formation may be a consequence of peroxide combination with carbon dioxide; this would likely confer increased solubility and yield powerful oxidizers. To address this topic, we utilized an anion-receptor solubilized form of the peroxide dianion<sup>12</sup> to elucidate the molecular level details of its reaction with carbon dioxide. As reported herein, we observed the formation of strongly oxidizing peroxy(di)-carbonate intermediates and studied their reaction with organic solvents to produce carbonate. In a complementary line of investigation, we showed that carbon dioxide activation of insoluble Li<sub>2</sub>O<sub>2</sub> similarly engenders solvent oxidation with the concomitant production of carbonate. Our findings shed light on the identity and behavior of the hot oxidants generated upon the facile and quantitative combination of O<sub>2</sub><sup>2-</sup> with CO<sub>2</sub> *via* direct spectroscopic detection and exploratory reaction chemistry.

### Results and discussion

#### Reaction of O<sub>2</sub><sup>2-</sup> with CO<sub>2</sub> using an anion receptor

Despite the drastic and deleterious effect that CO<sub>2</sub> has upon the performance of a cycling lithium–oxygen battery, our understanding of the chemical entities responsible for this effect is poor and based primarily upon computational studies or observation of terminal reaction products.<sup>2,8</sup> To examine the effect of CO<sub>2</sub> on the oxidative power of peroxide, an anion receptor complex<sup>13</sup> of the peroxide dianion, [O<sub>2</sub>C<sub>6</sub>mBDCA-5t-H<sub>6</sub>]<sup>2-</sup> (**1**, Fig. 1),<sup>12</sup> was employed as a soluble source of peroxide dianion. The anion receptor *m*BDCA-5t-H<sub>6</sub> encapsulates the peroxide dianion *via* six N–H⋯O hydrogen bonds. Since its

<sup>a</sup>Department of Chemistry, Massachusetts Institute of Technology, 77 Massachusetts Avenue, Cambridge, MA 02139-4307, USA. E-mail: ccummins@mit.edu; Tel: +1 617 253 5332

<sup>b</sup>Department of Chemistry, University of California, Davis, One Shields Avenue, Davis, CA 95616, USA

<sup>c</sup>Department of Chemistry, Queen's University, 90 Bader Lane, Kingston, Ontario K7L3N6, Canada

<sup>d</sup>Department of Chemistry and Chemical Biology, Harvard University, 12 Oxford Street, Cambridge, MA 02138, USA

† Electronic supplementary information (ESI) available: Full experimental, crystallographic and spectroscopic data. CCDC 1512972. For ESI and crystallographic data in CIF or other electronic format see DOI: 10.1039/c7sc01230f

‡ These authors contributed equally.

§ Current address: Centro de Investigaciones Químicas, IICBA, Universidad Autónoma del Estado de Morelos, Avenida Universidad 1001, Colonia Chamilpa, C.P. 62209, Cuernavaca, Morelos, Mexico.



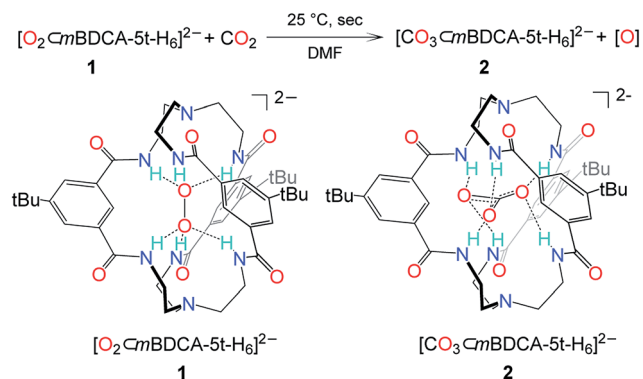


Fig. 1 The reaction scheme of peroxide cryptate **1** with  $\text{CO}_2$  and a line drawing of  $[\text{O}_2\text{CmBDCA-5t-H}_6]^{2-}$  and  $[\text{CO}_3\text{CmBDCA-5t-H}_6]^{2-}$ .

discovery, this cryptate has enabled exploration of the reactivity of the peroxide dianion with small molecules in polar organic media without the complicating influence of acidic protons.<sup>12,14</sup> Despite being a simple molecule, the peroxide dianion has yielded rich and previously unknown chemistry, including metal-free oxidation of carbon monoxide (CO) generating carbonate, which is encapsulated by the anion receptor as  $[\text{CO}_3\text{CmBDCA-5t-H}_6]^{2-}$  (**2**, Fig. 1).<sup>14</sup>

While the conversion of **1** to **2** under CO (1 atm, 40 °C) takes two hours to go to completion, exposing a dimethylformamide-*d*<sub>7</sub> (DMF-*d*<sub>7</sub>) solution of **1** to  $\text{CO}_2$  (1 atm, 25 °C) resulted in the essentially instantaneous formation of carbonate cryptate  $[\text{CO}_3\text{CmBDCA-5t-H}_6]^{2-}$  as indicated by <sup>1</sup>H NMR spectroscopy. Formation of  $\text{O}_2$  gas was not observed by gas chromatography (GC) analysis of the reactor headspace gases,<sup>15</sup> suggesting the possibility of oxygen incorporation into the solvent molecules. To probe the fate of the “missing oxygen atom” according to the equation at the top of Fig. 1, the reaction of  $\text{CO}_2$  and **1** was next performed in the presence of oxygen atom acceptors. While **1** on its own is unreactive towards  $\text{PPh}_3$  and methoxythioanisole at 25 °C, exposing a mixture of **1** and an organic oxygen-atom acceptor to  $\text{CO}_2$  (1 atm, 25 °C) resulted in the rapid formation of triphenylphosphine oxide (90%, Fig. 2) or 1-(methylsulfinyl)-4-methoxybenzene (61%, Fig. 2), respectively.

Aiming to establish the chemical identity of the oxidant(s) generated upon exposure of peroxide cryptate **1** to  $\text{CO}_2$ , we followed the reaction by variable temperature <sup>13</sup>C NMR spectroscopy. A strong new signal at  $\delta = 156.9$  ppm, together with one minor species resonating at  $\delta = 157.4$  ppm, was observed at -50 °C (Fig. 3). We first considered peroxy carbonate ( $^-\text{OOCO}_2^-$ , Fig. 3) and hydroperoxy carbonate ( $\text{HOOCO}_2^-$ , Fig. 3)



Fig. 2 Addition of  $\text{CO}_2$  to **1** in the presence of an oxygen-atom acceptor.

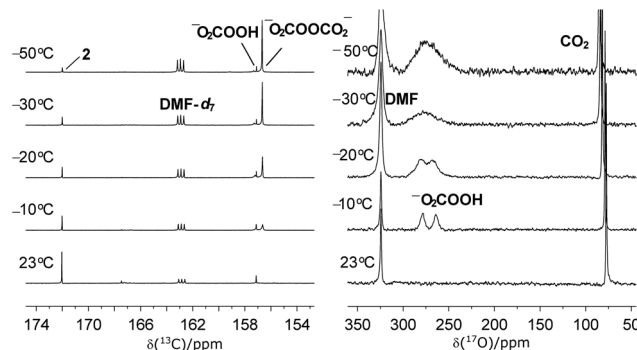


Fig. 3 Variable temperature <sup>13</sup>C NMR (left) and <sup>17</sup>O NMR (right) analysis of the reaction between <sup>13</sup> $\text{CO}_2$  and **1**.

as candidates to correspond to the observed <sup>13</sup>C NMR signals, since hydroperoxy carbonate is known to be active for sulfide oxidation.<sup>16,17</sup> The salt  $[\text{PPN}][\text{HOO}^{13}\text{CO}_2]$  (PPN = bis(triphenylphosphine)iminium), which was generated *in situ* from  $\text{H}_2\text{O}_2$  and bicarbonate  $[\text{PPN}][\text{H}^{13}\text{CO}_3]$  ( $\delta = 160.0$  ppm),<sup>18–20</sup> showed a single <sup>13</sup>C resonance at  $\delta = 157.5$  ppm, confirming the identity of the minor intermediate as  $\text{HOOCO}_2^-$ .

Moreover, <sup>13</sup>C Gauge-Independent Atomic Orbital (GIAO) NMR calculations of the chemical shifts of potential candidates were performed.<sup>15</sup> From a range of potential chemical species (Fig. 4), symmetric peroxydicarbonate ( $^-\text{O}_2\text{COOCO}_2^-$ ) emerged as the most plausible assignment for the major product at  $\delta = 156.9$  ppm, having the best match between the observed and calculated <sup>13</sup>C NMR chemical shift.<sup>15</sup> In an effort to independently generate  $^-\text{O}_2\text{COOCO}_2^-$ , an experiment was carried out in which excess <sup>13</sup> $\text{CO}_2$  was added to a frozen mixture of potassium *tert*-butoxide and bis(trimethylsilyl) peroxide giving rise to a single new <sup>13</sup>C NMR resonance at  $\delta = 155.5$  ppm (-40 °C), tentatively supporting our identification of the major **1** +  $\text{CO}_2$  product as symmetric peroxydicarbonate. Differences in the medium and reaction conditions may account for the observed chemical shift difference (155.5 ppm here *versus* 156.9 ppm, above). Similarly, superoxide ( $\text{O}_2^{\cdot-}$ ) has been documented to absorb two equivalents of  $\text{CO}_2$ , generating unsymmetrical peroxydicarbonate (Fig. 4) as a precipitate.<sup>21</sup> In our hands, the low

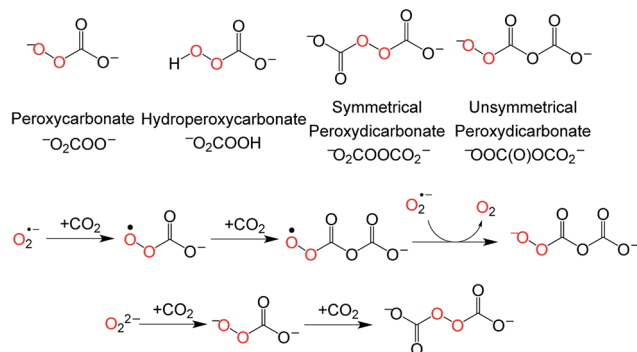


Fig. 4 Possible intermediates during the conversion of **1** and  $\text{CO}_2$  to **2** (top) and formation of symmetric and unsymmetric peroxydicarbonate (bottom).



solubility of this unsymmetrical peroxydicarbonate material precluded its characterization by solution  $^{13}\text{C}$  NMR studies under conditions we employed successfully for *in situ* characterization of  $^-\text{O}_2\text{COOCO}_2^-$  and  $\text{HOOCO}_2^-$ . This establishes that different oxidants are generated upon addition of  $\text{CO}_2$  to superoxide as compared with the peroxide dianion (Fig. 4).

Further support for the formation of  $\text{HOOCO}_2^-$  and  $^-\text{O}_2\text{COOCO}_2^-$  upon interaction of  $\text{CO}_2$  with peroxide sources was provided by variable temperature  $^{17}\text{O}$  NMR spectroscopy. Due to the fast relaxation times of  $^{17}\text{O}$  nuclei, observation of the  $^{17}\text{O}$  resonance for mid-size molecules such as  $1\text{-}^{17}\text{O}_2$  and  $2\text{-CO}^{17}\text{O}_2$  was expected to be challenging in solution.<sup>22</sup> Indeed,  $^{17}\text{O}$  NMR measurements of independently prepared peroxide cryptate  $1\text{-}^{17}\text{O}_2$  and carbonate cryptate  $2\text{-CO}^{17}\text{O}_2$  (70%,  $^{17}\text{O}$ -enriched) showed no resonances between  $\delta = -1100$  and  $+1800$  ppm ( $\text{H}_2\text{O}$  used as a reference,  $\delta = 0$  ppm) in DMF. However, solid-state  $^{17}\text{O}$  NMR measurements for  $1\text{-}^{17}\text{O}_2$  and  $2\text{-CO}^{17}\text{O}_2$  were successful, as reported previously in the case of  $2\text{-CO}^{17}\text{O}_2$ ,<sup>14</sup> and in the present work for  $1\text{-}^{17}\text{O}_2$ , providing the benchmark  $^{17}\text{O}$  NMR chemical shifts ( $\delta = 260$  ppm for  $1\text{-}^{17}\text{O}_2$  and  $170$  ppm for  $2\text{-CO}^{17}\text{O}_2$ ) (Fig. 5, Table 1). As seen in Fig. 3, 70%  $^{17}\text{O}$ -enriched samples of  $\text{HOOCO}_2^-$  and  $^-\text{O}_2\text{COOCO}_2^-$  generated in DMF solution at  $-78$  °C from the reaction of  $1\text{-}^{17}\text{O}_2$  and  $^{13}\text{CO}_2$  resulted in a broad  $^{17}\text{O}$  NMR resonance at  $\delta = 275.3$  ppm, assigned as overlapping signals of  $\text{HOOCO}_2^-$  and  $^-\text{O}_2\text{COOCO}_2^-$ . Upon gradual warming of the sample to  $-10$  °C, the intensity of the signal decayed; the signal ultimately resolved into two peaks with equal intensities at  $\delta = 278.7$  and  $264.0$  ppm, distinct from those observed for  $1\text{-}^{17}\text{O}_2$  and  $2\text{-CO}^{17}\text{O}_2$ . The two peaks observed are attributed to  $\text{HOOCO}_2^-$

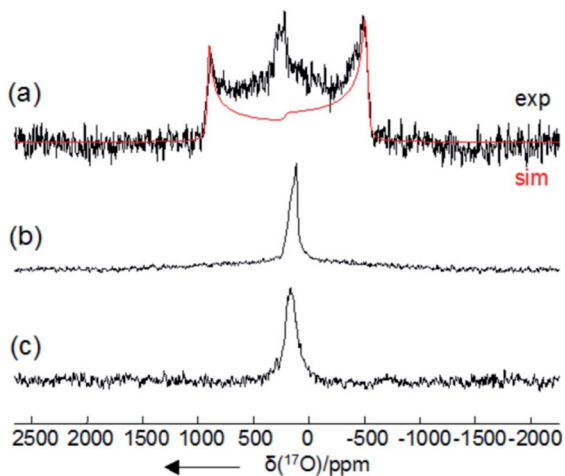


Fig. 5 Experimental (black trace) and simulated (red trace) solid-state  $^{17}\text{O}$  NMR spectra of (a)  $1\text{-}^{17}\text{O}_2$ , (b)  $2\text{-CO}^{17}\text{O}_2$ , and (c) product resulting from the treatment of solid  $1\text{-}^{17}\text{O}_2$  with  $\text{CO}_2$ . All solid-state  $^{17}\text{O}$  NMR experiments were performed on a Bruker Avance-600 (14.1 T) spectrometer under static conditions. A Hahn echo sequence was used for recording the static spectra to eliminate the acoustic ringing from the probe. A 4 mm Bruker MAS probe was used without sample spinning. The effective  $90^\circ$  pulse was of a duration of  $1.7$   $\mu\text{s}$ . High power  $^1\text{H}$  decoupling (70 kHz) was applied in all static experiments. A liquid  $\text{H}_2\text{O}$  sample was used for both RF power calibration and  $^{17}\text{O}$  chemical shift referencing ( $\delta = 0$  ppm).

which contains two chemically inequivalent  $^{17}\text{O}$  atoms ( $\delta = 278.7$  ppm for  $\text{HOOCO}_2^-$  and  $264.0$  ppm for  $\text{HOOCO}_2^-$ ), in contrast to the situation for  $^-\text{O}_2\text{COOCO}_2^-$  in which the peroxy oxygen atoms are related by symmetry. The appearance of the relatively sharp  $^{17}\text{O}$  NMR signals assigned to  $\text{HOOCO}_2^-$  coupled with the concurrent observation of monodeprotonated cryptand ( $[\text{mBDCA-5t-H}_5]^-$ )<sup>14</sup> by  $^1\text{H}$  NMR spectroscopy strongly suggests that  $\text{HOOCO}_2^-$  is not strongly sequestered inside the anion receptor. The observed  $^{17}\text{O}$  NMR chemical shifts are in accordance with expectations arising from  $^{17}\text{O}$  NMR absolute shielding calculations and compare well with data for benchmark organic compounds containing the peroxy functional group.<sup>23</sup>

### The mechanism of $\text{CO}_2$ /peroxide driven oxidation

Having thereby established the identity of the active oxidants generated from the combination of  $\text{O}_2^{2-}$  and  $\text{CO}_2$  as  $\text{HOOCO}_2^-$  and  $^-\text{O}_2\text{COOCO}_2^-$ , we next turned our attention to the mechanism of  $\text{CO}_2$ /peroxide driven oxidation. The reaction of  $^{18}\text{O}$ -labeled  $1$  and  $\text{CO}_2$  was performed in the presence of an oxidizable substrate. Exposure of a mixture of  $1\text{-}^{18}\text{O}_2$  and  $\text{PPh}_3$  to  $\text{CO}_2$  furnished  $^{18}\text{OPPh}_3$  as the oxidized product based on GCMS analysis.<sup>15</sup> The obtained  $^{18}\text{O}$  isotope labeling data precluded the possibility of O–O bond cleavage prior to the oxygen atom transfer (OAT) reaction, as such a process would yield isotopic scrambling and result in a mixture of  $^{16}\text{OPPh}_3$  and  $^{18}\text{OPPh}_3$ . Therefore,  $\text{H}^{18}\text{O}_2\text{CO}_2^-$  with its peroxy unit intact as it was derived from the peroxide dianion – is implicated as the active species for the OAT conversion of  $\text{PPh}_3$  to  $\text{OPPh}_3$  (Fig. 6, OAT pathway). In contrast, addition of  $\text{CO}_2$  to a solution of  $1\text{-}^{18}\text{O}_2$  in the presence of the hydrogen atom donor 9,10-dihydroanthracene (DHA) led to a statistical mixture of anthraquinone products with  $^{16}\text{O}$  and  $^{18}\text{O}$  incorporation.<sup>15</sup> The observed isotope scrambling was likely due to a sequence of H-atom abstraction/radical recombination reactions. By analogy to the behavior of organic peroxydicarbonates,<sup>26</sup> symmetrical peroxydicarbonate would be expected to undergo O–O bond homolysis generating two equivalents of the reactive carbonate radical  $\text{CO}_3^{\cdot-}$  (Fig. 6, hydrogen atom transfer (HAT) pathway).<sup>27</sup> Quantum chemical calculations indicate that homolytic cleavage of the O–O bond in  $^-\text{O}_2\text{COOCO}_2^-$  is only mildly endergonic (reaction free energy  $+14$  kcal mol $^{-1}$ ). This species thus has an unusually weak O–O bond.

Homolytic cleavage of the O–O bond and generation of  $\text{CO}_3^{\cdot-}$  appears to be favorable for two reasons: (i) repulsion of the negative charge due to poor solvation in organic solvents resulting in coulombic explosion<sup>28</sup> and (ii) resonance stabilization of the unpaired electron of the carbonate radical anion over the carbonate  $\pi$  system. Carbonate radicals have been generated previously *via* laser photolysis of aqueous persulfate in the presence of bicarbonate.<sup>29</sup> Carbonate radicals have been implicated in guanine oxidation<sup>27</sup> and are also believed to be formed upon treatment of peroxyxynitrite ( $\text{ONOO}^-$ ) with  $\text{CO}_2$ , and in that case generate nitrogen dioxide as a byproduct.<sup>27,30,31</sup> Furthermore, in the manganese-catalyzed oxidation of amino acids by  $\text{H}_2\text{O}_2$ , the formation of reactive oxygen species only



**Table 1** Experimental solid-state  $^{17}\text{O}$  NMR and ADF computational results on  $[\text{K}_2(\text{DMF})_3][^{17}\text{O}_2\text{C}m\text{BDCA-5t-H}_6]$ ,  $[\text{K}_2(\text{DMF})_3][\text{C}^{17}\text{O}_3\text{C}m\text{BDCA-5t-H}_6]$ , and related compounds

Compound		$\delta_{\text{iso}}^a/\text{ppm}$	$\delta_{11}/\text{ppm}$	$\delta_{22}/\text{ppm}$	$\delta_{33}/\text{ppm}$	$C_Q/\text{MHz}$	$\eta_Q/\text{MHz}$
1	Exp	260	335	335	110	-16.6	0.0
	ADF	308	388	388	148	-17.5	0.000
2	Exp	170	266	194	50	7.5	0.7
	ADF	223	335	222	112	7.03	0.95
$\text{O}_2^{2-}$	ADF	221	398	398	-13.3	-18.66	0.000
$\text{H}_2\text{O}_2$	Exp <sup>b</sup>	180	—	—	—	-16.31	0.687
	ADF	182	383	211	-48	-16.81	0.969
$\text{Li}_2\text{O}_2$	Exp <sup>c</sup>	227	352	352	-23	-18.66	0.00

<sup>a</sup> The uncertainties in the experimental data are:  $\delta_{\text{iso}} \pm 2$  ppm;  $\delta_{ii} \pm 10$  ppm;  $C_Q \pm 0.2$  MHz;  $\eta_Q \pm 0.1$ . <sup>b</sup> See ref. 24. <sup>c</sup> See ref. 25.

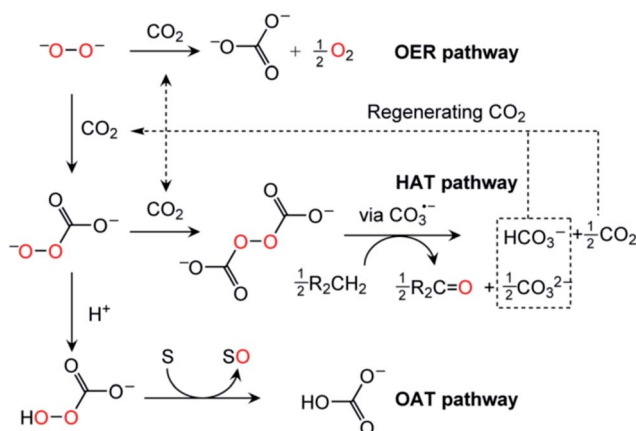


**Fig. 6** Proposed mechanistic pathways for  $\text{CO}_2$ -mediated solvent decomposition in lithium- $\text{O}_2$  batteries. OER is an "oxygen evolving reaction", HAT is a "hydrogen atom transfer" oxidative process involving hydrogen atom abstraction by carbonate radical anion, and OAT is "oxygen atom transfer" to a substrate, S.

occurred when  $\text{HCO}_3^-$  buffer was used.<sup>32,33</sup> Carbonate radicals generated in lithium-oxygen batteries can then engage in HAT reactions with solvents containing weak C-H bonds, driven by the high O-H bond strength ( $\text{BDE} \approx 107 \text{ kcal mol}^{-1}$ ) of the bicarbonate that is formed.<sup>27</sup> Accordingly, we suggest that for stability under lithium- $\text{O}_2$  cell cycling conditions, an organic solvent/electrolyte should have no C-H bonds of  $\text{BDE} \approx 107 \text{ kcal mol}^{-1}$  or less.

To experimentally confirm the generation of  $\text{CO}_3^{\bullet-}$ , **1** was treated with  $\text{CO}_2$  in the presence of the spin trap 5-tert-butoxycarbonyl-5-methyl-1-pyrroline-N-oxide (BMPO), and the reaction was monitored by EPR spectroscopy.<sup>34</sup> Upon addition of the  $\text{CO}_2$ , signals for the hydroxyl adduct  $[\text{BMPO-OH}]^{\bullet}$  together with small quantities (*ca.* 5%) of an unidentified spin-trap adduct suspected to be  $[\text{BMPO-OCO}_2]^{\bullet-}$  were observed within seconds (Fig. 7). Formation of  $[\text{BMPO-OH}]^{\bullet}$  is proposed to occur *via* a rapid reaction between the chemically generated  $\text{CO}_3^{\bullet-}$  and BMPO, initially yielding  $[\text{BMPO-OCO}_2]^{\bullet-}$ , followed by decarboxylation and protonation. The proton source under these conditions could be the anion receptor *m*BDCA-5t- $\text{H}_6$  (Fig. 7C). This sequence is directly along the lines proposed for the related spin trap DMPO under exposure to carbonate

radicals.<sup>35,36</sup> On longer timescales,  $[\text{BMPO-OH}]^{\bullet}$  was further oxidized to  $[\text{BMPO-O}]^{\bullet}$  and other unidentified decomposition products.<sup>34</sup>

### Activation of solid $\text{Li}_2\text{O}_2$ with $\text{CO}_2$ in aprotic organic media

To examine the effect of  $\text{CO}_2$  on the oxidative power of  $\text{Li}_2\text{O}_2$  under conditions relevant to the charging of lithium-air cells, commercially available solid  $\text{Li}_2\text{O}_2$  was exposed to  $\text{CO}_2$  (1 atm,  $25^\circ\text{C}$ , 48 h) in 1,2-dimethoxyethane (DME). In contrast to the results from the control experiments carried out similarly but in the absence of  $\text{CO}_2$ , substantial amounts of methyl methoxyacetate were identified among the products of DME oxidation (Fig. 8). Approximately 51% of the  $\text{Li}_2\text{O}_2$  was consumed, and quantitative conversion of the consumed  $\text{Li}_2\text{O}_2$  to  $\text{Li}_2\text{CO}_3$  (based upon lithium) was observed by  $^{13}\text{C}$  NMR spectroscopy and total inorganic carbonate (TIC) analysis.<sup>15</sup> The consumed peroxide must generate an oxidizing equivalent; 74% was identified as

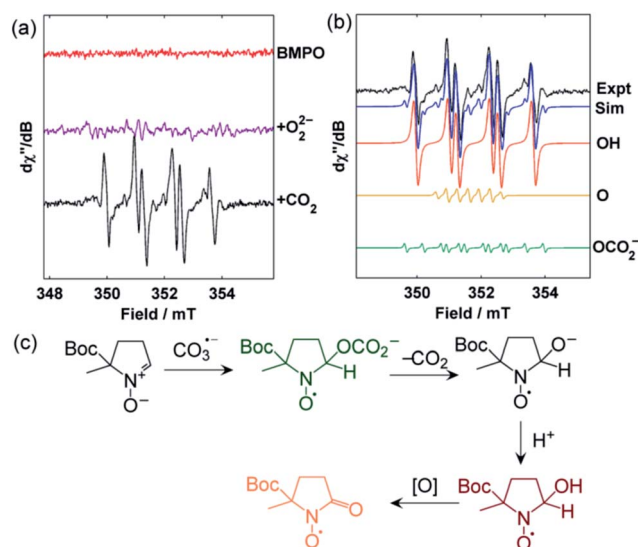


**Fig. 7** (a) X-Band EPR spectra of: pristine BMPO in DMF (red), BMPO + **1** without adding  $\text{CO}_2$  in DMF (purple), and exposure of BMPO + **1** to  $\text{CO}_2$  in DMF (black). (b) Simulation of the EPR spectra of BMPO + **1** +  $\text{CO}_2$  in DMF by linear combination of the contribution from:  $[\text{BMPO-OCO}_2]^{\bullet-}$  (green),  $[\text{BMPO-OH}]^{\bullet}$  (red), and  $[\text{BMPO-O}]^{\bullet}$  (yellow). (c) Formation of  $[\text{BMPO-O}]^{\bullet}$  from  $[\text{BMPO-OH}]^{\bullet}$  and an oxidant "[O]".





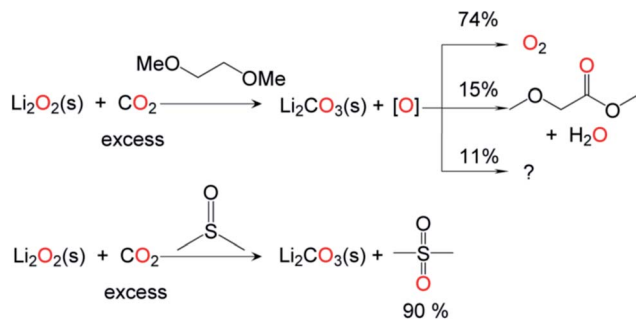


Fig. 8  $\text{CO}_2$ -mediated oxidation of organic solvents by  $\text{Li}_2\text{O}_2$ . Addition of excess  $\text{CO}_2$  to solid  $\text{Li}_2\text{O}_2$  in the organic solvent 1,2-dimethoxyethane (DME) generates an oxidizing equivalent "O", which converts to  $\text{O}_2$  (74%) and methyl methoxyacetate (15%) with the remainder unidentified. A similar reaction performed in dimethylsulfoxide (DMSO) generated dimethylsulfone (DMSO<sub>2</sub>) in a 90% yield.

evolved  $\text{O}_2$  and 15% as methyl methoxyacetate (Fig. 8), with the remainder unidentified. We also introduced solid  $\text{Li}_2\text{O}_2$  into neat DMSO under a  $\text{CO}_2$  atmosphere (1 atm, 25 °C, 48 h), given the reported use of DMSO in lithium- $\text{O}_2$  cells.<sup>37</sup> More than 90% of the  $\text{Li}_2\text{O}_2$  consumed participated in the conversion of DMSO to DMSO<sub>2</sub> (Fig. 8). Viewed in the context of cycling lithium- $\text{O}_2$  cells, the rate of  $\text{CO}_2$ -induced solvent decomposition in bona fide lithium-air cells is perhaps lower than that observed in the current study due to the difference in  $\text{CO}_2$  partial pressures. Nonetheless, considering the low cycling rate and long cycling time of a typical lithium-air battery,<sup>38</sup> our findings highlight that extensive oxidative degradation of the electrolyte in a cell will occur during cell cycling even when a small amount of  $\text{CO}_2$  is introduced or otherwise generated in the system.<sup>39</sup> During cell cycling,  $\text{CO}_2$  is generated at the surface of lithium peroxide-impregnated carbon electrodes,<sup>39</sup> leading us to speculate that the proposed chemistry (Fig. 8) should be expected to occur on a polarized electrode/electrolyte interface as well. It should be noted that while commercial  $\text{Li}_2\text{O}_2$  was used in the present study, it is conceivable that the varied morphologies of electrochemically generated  $\text{Li}_2\text{O}_2$  may react with  $\text{CO}_2$  at different rates. Due to the preponderance of conditions which result in varied  $\text{Li}_2\text{O}_2$  crystallinity, size and surface structure,<sup>40,41</sup> commercial  $\text{Li}_2\text{O}_2$  was chosen as an ideal benchmark reactant with  $\text{CO}_2$ .

A recent publication reported that when present in a charging lithium-air cell (>3.5 V vs.  $\text{Li}^+/\text{Li}$ ), the secondary amine 2,2,6,6-tetramethyl-4-piperidone (4-oxo-TEMP) was converted to the oxyl amine radical 4-oxo-TEMPO, as confirmed by EPR spectroscopy. 4-oxo-TEMP has been used in the past as a trap for singlet oxygen, leading the authors to propose that singlet oxygen was responsible for the observed conversion.<sup>10</sup> An alternative explanation for the production of 4-oxo-TEMPO involves the oxidants being generated by activating  $\text{Li}_2\text{O}_2$  with  $\text{CO}_2$ , considering that the onset potential of  $\text{CO}_2$  formation in a typical lithium-air cell is also 3.5 V.<sup>42</sup> Accordingly, we found that exposing  $\text{Li}_2\text{O}_2$  to  $\text{CO}_2$  (1 atm, 25 °C, 24 h) in the same solvent and electrolyte as described in the literature, but without the application of an electrode potential, also resulted

in the formation of 4-oxo-TEMPO. Of the oxidizing equivalents generated during the transformation of  $\text{Li}_2\text{O}_2$  to  $\text{Li}_2\text{CO}_3$ , ca. 15% were incorporated into the 4-oxo-TEMPO reaction product based on EPR spin quantification. These experiments suggest that the oxidation of 4-oxo-TEMP is most likely due to  $\text{CO}_2$ /peroxide-derived oxidants as opposed to singlet oxygen formation or at the very least that 4-oxo-TEMP is not a selective probe for singlet oxygen in  $\text{Li}-\text{O}_2$  cells under conditions of  $\text{CO}_2$  availability.

## Conclusions

While previous studies on lithium- $\text{O}_2$  batteries have attributed the low cycling number and capacity fading to singlet oxygen<sup>10</sup> and superoxide,<sup>4-7</sup> it is now clear that  $\text{CO}_2$ /peroxide-derived oxidants are responsible for carbonate formation by way of the active oxidants  $\text{HOOCO}_2^-$  and  $\text{CO}_3^{\cdot-}$  via  $^-\text{O}_2\text{COOCO}_2^-$ . Since prototypical lithium-air cells (ether electrolyte, carbon cathode) lose 5–7% of their capacity to parasitic  $\text{CO}_2$  formation per complete cycle<sup>39</sup> and have a typical cycling number of ca. 50, the resulting  $\text{CO}_2$ /peroxide dianion-derived oxidants were expected to cause organic electrolyte degradation. This oxidative degradation may occur both during discharge through reaction of the peroxide dianion with  $\text{CO}_2$  and during recharge through electrochemical oxidation of carbonate initially generating the carbonate radical ( $\text{CO}_3^{\cdot-}$ ). It has been established that recharging a lithium- $\text{O}_2$  battery regenerates  $\text{CO}_2$  from  $\text{Li}_2\text{CO}_3$ , however identification of the mechanism and product(s) of electrochemical  $\text{Li}_2\text{CO}_3$  degradation have been unclear.<sup>2</sup> Our studies provide evidence for a mechanistic pathway by which carbonate radical anions, when generated, engage in C-H abstraction from the solvent (C-H bond  $\cong$  107 kcal mol<sup>-1</sup>, or less)<sup>27</sup> and lead to solvent degradation and reformation of  $\text{CO}_2$  (Fig. 6). The regenerated  $\text{CO}_2$  sets in motion a decomposition cycle, therefore if even a small percentage of the total  $\text{Li}_2\text{O}_2$  is converted to  $\text{CO}_2$ , extensive oxidative degradation of the electrolyte in a cell will occur over the course of many cycles. If  $\text{CO}_2$  cannot be excluded from these systems then it is critical that the electrolyte and other cell components are invulnerable to reactive  $\text{CO}_2$ /peroxide-derived oxidants if the full potential of rechargeable lithium- $\text{O}_2$  battery systems is to be realized.

## Acknowledgements

This publication is based on work funded by the Robert Bosch Company and the National Science Foundation under CHE-1305124. The EPR spectroscopy in this study was funded by the National Science Foundation under CHE-1305124. We thank Carl Brozek, Ioana Knopf, Wesley Transue and Chong Liu for assistance with the instrumentation. We thank Prof. Yogesh Surendranath (MIT) for helpful discussion.

## References

- 1 P. G. Bruce, S. A. Freunberger, L. J. Hardwick and J.-M. Tarascon, *Nat. Mater.*, 2011, **11**, 172.



- 2 S. R. Gowda, A. Brunet, G. M. Wallraff and B. D. McCloskey, *J. Phys. Chem. Lett.*, 2013, **4**, 276–279.
- 3 H.-K. Lim, H.-D. Lim, K.-Y. Park, D.-H. Seo, H. Gwon, J. Hong, W. A. Goddard, H. Kim and K. Kang, *J. Am. Chem. Soc.*, 2013, **135**, 9733–9742.
- 4 S. A. Freunberger, Y. Chen, Z. Peng, J. M. Griffin, L. J. Hardwick, F. Bardé, P. Novák and P. G. Bruce, *J. Am. Chem. Soc.*, 2011, **133**, 8040–8047.
- 5 Y. Chen, S. A. Freunberger, Z. Peng, F. Bardé and P. G. Bruce, *J. Am. Chem. Soc.*, 2012, **134**, 7952–7957.
- 6 D. G. Kwabi, T. P. Batcho, C. V. Amanchukwu, N. Ortiz-Vitoriano, P. Hammond, C. V. Thompson and Y. Shao-Horn, *J. Phys. Chem. Lett.*, 2014, **5**, 2850–2856.
- 7 M. M. O. Thotiyl, S. A. Freunberger, Z. Peng and P. G. Bruce, *J. Am. Chem. Soc.*, 2013, **135**, 494–500.
- 8 S. Yang, P. He and H. Zhou, *Energy Environ. Sci.*, 2016, **9**, 1650–1654.
- 9 X. Yao, Q. Dong, Q. Cheng and D. Wang, *Angew. Chem., Int. Ed.*, 2016, **55**, 11344–11353.
- 10 J. Wandt, P. Jakes, J. Granwehr, H. A. Gasteiger and R.-A. Eichel, *Angew. Chem., Int. Ed.*, 2016, **55**, 6892–6895.
- 11 C. W. Jones and J. H. Clark, Introduction to the preparation and properties of hydrogen peroxide, *R. Soc. Chem.*, 1999, 1–36.
- 12 N. Lopez, D. J. Graham, R. McGuire, G. E. Alliger, Y. Shao-Horn, C. C. Cummins and D. G. Nocera, *Science*, 2012, **335**, 450–453.
- 13 The CAS registry number of the anion receptor is: 1360563-21-8.
- 14 M. Nava, N. Lopez, P. Muller, G. Wu, D. G. Nocera and C. C. Cummins, *J. Am. Chem. Soc.*, 2015, **137**, 14562–14565.
- 15 See ESI.†
- 16 D. A. Bennett, H. Yao and D. E. Richardson, *Inorg. Chem.*, 2001, **40**, 2996–3001.
- 17 D. E. Richardson, H. Yao, K. M. Frank and D. A. Bennett, *J. Am. Chem. Soc.*, 2000, **122**, 1729–1739.
- 18 D. P. Jones and W. P. Griffith, *J. Chem. Soc., Dalton Trans.*, 1980, 2526–2532.
- 19 J. Flangan, D. P. Jones, W. P. Griffith, A. C. Skapski and A. P. West, *J. Chem. Soc., Chem. Commun.*, 1986, 20–21.
- 20 M. G. Bonini, S. A. Gabel, K. Ranguelova, K. Stadler, E. F. DeRose, R. E. London and R. P. Mason, *J. Biol. Chem.*, 2009, **284**, 14618–14627.
- 21 J. L. Roberts, T. S. Calderwood and D. T. Sawyer, *J. Am. Chem. Soc.*, 1984, **106**, 4667–4670.
- 22 I. P. Gerothanassis, in *Encyclopedia of Magnetic Resonance*, 2011, pp. 1–15.
- 23 G. Cerioni and F. Mocci, *<sup>17</sup>O NMR Spectroscopy of Organic Compounds Containing the –O–O– group*, John Wiley & Sons, Ltd, 2009.
- 24 J. Lu, X. Kong, V. Terskikh and G. Wu, *J. Phys. Chem. A*, 2015, **119**, 8133–8138.
- 25 M. Leskes, N. E. Drewett, L. J. Hardwick, P. G. Bruce, G. R. Goward and C. P. Grey, *Angew. Chem., Int. Ed.*, 2012, **51**, 8560–8563.
- 26 W. A. Strong, *Ind. Eng. Chem.*, 1964, **56**, 33–38.
- 27 N. B. Surmeli, K. L. Nadia, A.-F. Miller and J. T. Groves, *J. Am. Chem. Soc.*, 2010, **132**, 17174–17185.
- 28 D. A. Armstrong, W. L. Waltz and A. Rauk, *Can. J. Chem.*, 2006, **84**, 1614–1619.
- 29 R. E. Huie, C. L. Clifton and P. Neta, *Radiat. Phys. Chem.*, 1991, **38**, 477–481.
- 30 S. V. Lymar and J. K. Hurst, *J. Am. Chem. Soc.*, 1995, **117**, 8867–8868.
- 31 M. G. Bonini, R. Radi, F.-S. Gerardo, A. M. D. C. Ferreira and O. Augusto, *J. Biol. Chem.*, 1999, **274**, 10802–10806.
- 32 B. S. Berlett, P. B. Chock, M. B. Yim and E. R. Stadtman, *Proc. Natl. Acad. Sci. U. S. A.*, 1990, **87**, 389–393.
- 33 M. B. Yim, B. S. Berlett, P. B. Chock and E. R. Stadtman, *Proc. Natl. Acad. Sci. U. S. A.*, 1990, **87**, 394–398.
- 34 H. Zhao, J. Joseph, H. Zhang, H. Karoui and B. Kalyanaraman, *Free Radical Biol. Med.*, 2001, **31**, 599–606.
- 35 D. B. Medinas, G. Cerchiaro, D. F. Trindade and O. Augusto, *IUBMB Life*, 2007, **59**, 255–262.
- 36 F. A. Villamena, E. J. Locigno, A. Rockenbauer, C. M. Hadad and J. L. Zweier, *J. Phys. Chem. A*, 2007, **111**, 384–391.
- 37 Z. Peng, S. A. Freunberger, Y. Chen and P. G. Bruce, *Science*, 2012, **337**, 563–566.
- 38 D. Aurbach, B. D. McCloskey, L. F. Nazar and P. G. Bruce, *Nat. Energy*, 2016, **1**, 16128.
- 39 B. D. McCloskey, A. Speidel, R. Scheffler, D. C. Miller, V. Viswanathan, J. S. Hummelshoj, J. K. Nørskov and A. C. Luntz, *J. Phys. Chem. Lett.*, 2012, **3**, 997–1001.
- 40 S. Lau and L. A. Archer, *Nano Lett.*, 2015, **15**, 5995–6002.
- 41 R. R. Mitchell, B. M. Gallant, Y. Shao-Horn and C. V. Thompson, *J. Phys. Chem. Lett.*, 2013, **4**, 1060–1064.
- 42 Y.-C. Lu, E. J. Crumlin, T. J. Carney, L. Baggetto, G. M. Veith, N. J. Dudney, Z. Liu and Y. Shao-Horn, *J. Phys. Chem. C*, 2013, **117**, 25948–25954.

